Applied Catalysis B: Environmental 200 (2017) 174–181

Contents lists available at ScienceDirect

Applied Catalysis B: Environmental

journal homepage: www.elsevier.com/locate/apcatb

Grafting doped manganite into nickel anode enables efficient and durable energy conversions in biogas solid oxide fuel cells

Bin Hua[a,*,1], Meng Li[b,1], Yi-Fei Sun[a], Ya-Qian Zhang[a], Ning Yan[c], Jian Li[b], Thomas Etsell[a], Partha Sarkar[d], Jing-Li Luo[a,*]

[a] Department of Chemical and Materials Engineering, University of Alberta, Edmonton, Alberta T6G 1H9, Canada
[b] School of Materials Science and Engineering, Huazhong University of Science and Technology, Wuhan, Hubei 430074, China
[c] Van't Hoff Institute for Molecular Sciences (HIMS), University of Amsterdam, Amsterdam, 1098XH, The Netherlands
[d] Environment & Carbon Management Division, Alberta Innovates-Technology Futures, Edmonton, Alberta T6N 1E4, Canada

ARTICLE INFO

Article history:
Received 12 May 2016
Received in revised form 27 June 2016
Accepted 1 July 2016
Available online 2 July 2016

Keywords:
Solid oxide fuel cell
Ni-based anode
$PrBaMn_2O_{5+\delta}$ perovskite
Sulfur tolerance
Carbon deposition resistance

ABSTRACT

Biogas, consisting of CH_4, CO_2 and a small amount of H_2S, is one of the most promising alternative energy sources. Solid oxide fuel cells (SOFCs) are ideal technologies to efficiently utilize biogas for producing electricity and heat. However, this is precluded because the conventional Ni-Y_2O_3 stabilized ZrO_2 (Ni-YSZ) anode for SOFC is inclined to cause carbon formation as well as to form inert and non-conductive S-containing species in biogas. To directly utilize the biogas in SOFC, a hybrid anode material, combining the slightly compromised merits of the conventional Ni-YSZ cermet and the alternative anode, i.e., $PrBaMn_2O_{5+\delta}$ perovskite oxide, is developed in this study. The $PrBaMn_2O_{5+\delta}$ dramatically resists the carbon formation and S adsorption on Ni surface and at the same time, it serves as the CO_2-captor, oxygen source and the medium for O^{2-} diffusion to accelerate both the carbon removal and S desorption processes. At 800 °C, the peak power density of the cell with the hybrid anode attains 1.35 W cm^{-2} in biogas, and no significant degradation is observed during the stability test. The hybrid anode, therefore, displays excellent activity, superior coke/sulfur resistance and stability in biogas, offering a promising technology for biogas utilization.

1. Introduction

The gradual depletion of fossil fuels necessitates the worldwide efforts to seek sustainable energy sources to meet our future energy needs. In this context, the development of new technologies that drive this progress for new energy sources exploration and/or efficient energy utilization becomes more crucial [1–4]. Biogas is one of the most promising alternative energy sources due to the advantages of its abundance and renewability [5–7]. Thus, technologies tailored to efficiently utilize it for producing electricity, heat and fuels draw growing attentions. The primary components of biogas are methane (CH_4) and inert carbonic gas (CO_2), and a small amount of hydrogen sulfide (H_2S) and others. Solid oxide fuel cell (SOFC) is one of the potential technologies for biogas utilization due to its merits of energy efficiency and fuel flexibility [1,8]. It is a promising process to directly convert the biogas into electricity by a SOFC stack without one-site purification process. Although the state of art SOFC exhibits excellent electrochemical performance and stability in H_2, direct utilization of biogas as the fuel in SOFC is precluded by the reason that the most commercialized Ni-Y_2O_3 stabilized ZrO_2 (Ni-YSZ) anode is inclined to induce carbon formation as well as to form inert and non-conductive S-containing species in CH_4 and H_2S (denoted as "sour" condition) fuels [9–11]. Numerous studies have now shown that the presence of CO_2 (denoted as "dry" condition) may mitigate the issue raised by carbon depositions for direct biogas SOFC [1,12], but it will initiate other concerns that impede the operation of a SOFC stack, e.g., fuel dilution and thermal stress.

In fact, to directly utilize the sour hydrocarbons in SOFCs, a large number of researchers have focused on the exploration of ceramic alternatives, e.g., perovskite-type compounds [13–21], which have outstanding carbon deposition resistance and H_2S tolerance. Generally, these single phase anode materials are mixed ionic-electronic conductors (MIECs). The electrochemical reaction sites for these anodes, therefore, are extended from the fuel/oxygen-conductor/electronic-conductor triple-phase boundaries (TPBs) to the MIECs/fuel double-phase boundaries (DPBs).

* Corresponding authors.
E-mail addresses: bhua1@ualberta.ca (B. Hua), jingli.luo@ualberta.ca (J.-L. Luo).
[1] These authors contributed equally to this work.

http://dx.doi.org/10.1016/j.apcatb.2016.07.001
0926-3373/

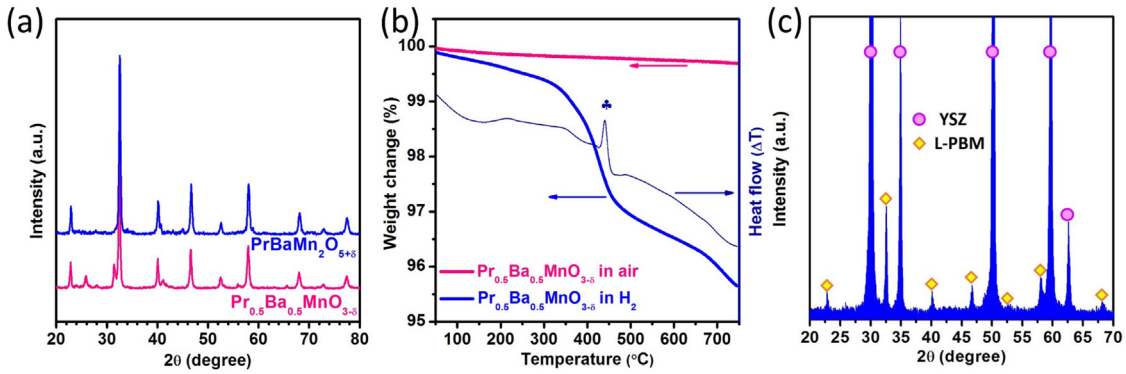

Fig. 1. (a) X-ray diffraction patterns of $Pr_{0.5}Ba_{0.5}MnO_{3-\delta}$ and $PrBaMn_2O_{5+\delta}$; (b) Thermogravimetric/Differential Thermal Analysis (TG/DTA) spectra of $Pr_{0.5}Ba_{0.5}MnO_{3-\delta}$ in air and in H_2; (c) X-ray diffraction pattern of YSZ and $PrBaMn_2O_{5+\delta}$ mixture after calcination at 950 °C in H_2 for 10 h. (For interpretation of the references to colour in the text, the reader is referred to the web version of this article.)

Although these ceramic anodes always show superior carbon deposition resistance and H_2S tolerance [19–21], their activities are only comparable with that of conventional Ni-YSZ anode at high temperatures (>850 °C). For example, the maximum power density of a single cell based on the $SrTi_{0.3}Fe_{0.7}O_{3-\delta}$ + Gd-doped-CeO_2 anode is only 337 mW cm^{-2} at 800 °C in H_2 [14], which is not high enough for the practical application. Since the trend in the development of SOFC system is to reduce the operation temperatures (<800 °C), the insufficient catalytic activity becomes the key obstacle for the implementation of these perovskite anodes [17,22,23]. Numerous scientists, thus, have attempted to optimize the electrochemical activities of these alternative anodes by doping elements [19–23] and/or infiltration metal catalysts [22,23]. The single cell with the $PrBaMn_2O_{5+\delta}$ anode demonstrated good catalytic activity and stability in H_2S containing CH_4 [21]. Although the kinetics of fuel oxidation process on them were dramatically improved, they are still not compatible to the single cells with anode supported architecture in the commercialized SOFC technology. It thus becomes critical to explore other effective methods to improve the carbon deposition resistance and H_2S tolerance of the anode without sacrificing the activity as well as the compatibility with the commercialized SOFC technologies.

Reasonably, a hybrid anode material which combines the merits of the Ni-YSZ and perovskite oxides should be developed. However, the fabrication process of conventional Ni-YSZ/YSZ cells is always accompanied by the high temperature (above 1350 °C) sintering process, which makes the incorporation of the perovskite oxides a difficult procedure [22,23]. Surface modification through infiltration is a widely adopted technology in SOFC research work [24–26]. It offers a low temperature fabrication technology for the proposed hybrid anode material. In this study, a conventional Ni-YSZ anode was modified by infiltrating a novel $PrBaMn_2O_{5+\delta}$ perovskite oxide, which has recently been proved as a highly active and coke/sulfur tolerant anode for sour hydrocarbon fueled SOFC [21]. It has been shown that the optimized SOFC displayed excellent activity and adequate coke/sulfur resistance, demonstrating a promising and practical approach towards direct biogas utilization.

2. Experimental

2.1. Material preparation and button cell fabrication

The anode supported cells were fabricated via tape-casting, screen-printing and co-sintering processes. Fabrication details have been well described in our previous work [8]. Specifically, the SOFC button cell (ϕ13 × 1 mm) consists of a Ni-YSZ supported anode (~1 mm), a Ni-YSZ functional anode (~10 μm), a YSZ electrolyte (~10 μm), a $Ce_{0.9}Gd_{0.1}O_{1.9}$ (GDC) barrier layer (~2 μm) and a $La_{0.8}Sr_{0.2}Co_{0.8}Fe_{0.2}O_{3-\delta}$ (LSCF)-GDC cathode (30 μm, 0.5 cm^2). As for the cell infiltrated with the layered perovskite, i.e., $PrBaMn_2O_{5+\delta}$ (L-PBM) nanoparticles (NPs), a solution containing stoichiometric $Pr(NO_3)_3{\cdot}5H_2O$, $Ba(NO_3)_2$ and $Mn(NO_3)_2{\cdot}4H_2O$ with ethylene glycol/citric acid added as the chelating agent was infiltrated into the Ni-YSZ anode, followed by firing at 950 °C for 5 h until the weight gain of the cell attained 3 wt.%. The L-PBM was obtained by reducing the simple perovskite $Pr_{0.5}Ba_{0.5}MnO_{3-\delta}$ (PBM) in H_2 at 800 °C for 4 h. The two types of cells are denoted as Ni-YSZ and NPs + Ni-YSZ, respectively.

2.2. Evaluation of the chemical performance

Since the main components of biogas are CH_4 and CO_2, the catalytic activities of the anode towards methane dry reforming reaction would dramatically affect the electrochemical performance of the cell. Thus, the dry reforming catalytic activities of Ni-YSZ (57:43 wt%, pre-sintered at 1390 °C to simulate the Ni-YSZ anode) and 3 wt.% LP-PBM infiltrated Ni-YSZ were compared. The measurements of the DRM activity were performed on a fixed bed reactor using a mixture of 0.2 g anode powder and 0.4 g inert quartz powder (SiO_2) as the catalyst. The packed reactor was then heated to 800 °C in H_2 and reduced for 5 h prior to the test. Then, an equal amount of CH_4 and CO_2 was fed into the reactor at the total flow rate of 20 ml min^{-1}. The DRM reactions took place at the temperatures between 700 and 800 °C. The effluent gases were collected and analyzed in a gas chromatography equipment (GC, Hewlett Packard Series two). The values of CH_4 conversion and CO selectivity were calculated according to Eqs. (1) and (2), respectively.

$$CH_4\text{conversion} = \frac{[CH_4]\,\text{outlet}}{[CH_4]\,\text{inlet}} \times 100\% \quad (1)$$

$$\text{COselectivity} = \frac{[CO]\,\text{outlet}}{[CO]\,\text{outlet} + [CO_2]\,\text{outlet}} \times 100\% \quad (2)$$

2.3. Evaluation of the electrochemical performance

Au paste (Heraeus Group) was brush painted on both the anode and cathode, and then calcined at 800 °C in air for 2 h. Pt mesh and wire (Sino-Platinum Metals CO.) were used as the current collector and measuring lead, respectively. SOFC cells were sealed on an alumina tube by using a Ceramabond® (Type 552) glass sealant and in-situ reduced in H_2 at 800 °C before the test. Current density-voltage (J-V) polarization curves and electrochemical impedance spectra (EIS) in H_2 (pure, 40 ml min^{-1}), dry CH_4 (CO_2:CH_4 = 1:1, 20 ml min^{-1}), sour H_2 (H_2 balanced with 50 ppm H_2S, 40 ml min^{-1}) and simulated biogas (CO_2:CH_4 = 1:1 and balanced with 50 ppm

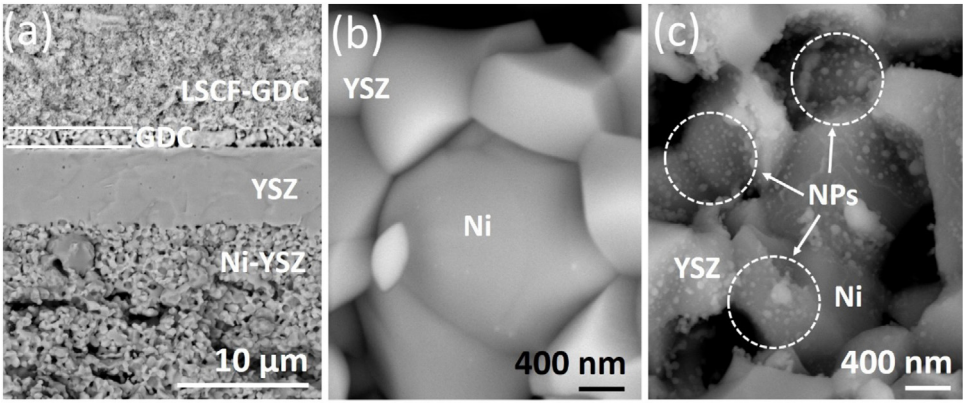

Fig. 2. (a) Cross-sectional microstructure of the anode/electrolyte/cathode triple-layers; (b) magnification of the as-reduced Ni-YSZ anode; (c) magnification of the $PrBaMn_2O_{5+\delta}$ infiltrated Ni-YSZ anode.

H_2S, 20 ml min^{-1}) were collected. The performance and stability of the cells in the dry CH_4 and sour H_2 were tested to estimate the carbon deposition resistance and sulfur tolerance separately before evaluating the cells in biogas. The biogas used in this study is equal amount of CO_2 and CH_4 balanced with 50 ppm H_2S, which is a typical composition used in the SOFC test. The performance stabilities of the cells in various atmospheres were also measured under 1 A cm^{-2} or 1.5 A cm^{-2} and at 800 °C. During the test, the LSCF-GDC cathode was fed with 500 ml min^{-1} fresh air.

2.4. Characterizations

The X-ray diffraction (XRD) patterns of the powders were identified by using Cu Kα radiation at a tube voltage of 40 kV and a tube current of 44 mA in a Rigaku Rotaflex equipment. The 2θ range was changing from 20° to 80° at 1 ° min^{-1}. An SDT-Q600 (TA instrument, USA) machine was used to carry out the thermogravimetry analysis (TGA) experiments. The gas flow rate during the TGA test was 50 ml min^{-1}. The microstructures of the cells before and after test were examined using field emission scanning electron microscopy (FESEM, Zeiss Sigma 300 VP). The carbon depositions were investigated by using temperature programmed oxidation (TPO) [TPO via coupled TGA-Mass Spectrometer (MS, Pfeiffer Vacuum GmbH)] method.

3. Results and discussions

As the XRD patterns of the as-prepared PBM (pink) shown in Fig. 1a, it is seen that the simple perovskite structure formed without any evidence of impurities after annealing at 950 °C for 5 h. Although the simple perovskite structure was very stable during the calcination in air (Fig. 1b, pink), the PBM demonstrated remarkable weight loss (loss of lattice oxygen) and a sharp exothermic peak (at 440 °C) upon heating in reducing atmosphere (Fig. 1b, blue). This exothermic process was accompanied by the crystal structure change (see XRD in Fig. 1, blue) from simple perovskite, i.e., -[$(Pr/BaO)_x$-MnO_2-$(Pr/BaO)_x$]- to layered structure, i.e., -[PrO_x-MnO_2-BaO-MnO_2-PrOx]-. The obtained L-PBM has been proved as a highly conductive, active and coke/sulfur tolerant anode material, which is probably the most advanced alternative anode for direct sour hydrocarbon SOFCs up to date [21]. Importantly, the L-PBM also shows good chemical compatibility with the YSZ. Fig. 1c demonstrates the XRD pattern of L-PBM/YSZ mixture calcined at 950 °C for 10 h. No impurities were detected, suggesting the two oxides are chemically compatible under the SOFC operation condition.

Before the electrochemical test, the SOFC cells were heated up to 800 °C in 10 mol% H_2–90 mol% N_2 and in-situ reduced in H_2 at 800 °C for 4 h. As the cross-sectional microstructure of the reduced full cell in Fig. 2a shows, the porous Ni-YSZ anode was well adhered to the dense YSZ electrolyte, which was approximately ~12 μm in thickness. The reduction of NiO in the anode generated a significant amount of pores for fuel gas to permeate through, and large areas of TPBs to carry out electrochemical reaction. Besides, the porous LSCF-GDC cathode also showed good coherence to the anode/electrolyte substrate after sintering at 950 °C. Comparing to the Ni-YSZ anode (Fig. 2b), the optimized anode (Fig. 2c) showed the presence of multiple L-PBM NPs with the sizes of ~50 nm. The Energy-dispersive X-ray (EDX) spectroscopy (Fig. 3) proved that the infiltrated L-PBM NPs were well distributed in the porous Ni-YSZ scaffold without significant agglomerations, which ensured the construction of an ideal hybrid anode. These active L-PBM NPs dramatically increased the electrochemically-active sites, and even rendered the YSZ surfaces able to catalyze the fuel oxidation reactions.

Based on the SEM observations, it is speculated that the infiltration of L-PBM NPs will improve the anode performance because the electrochemically-active areas are increased. As a benchmark, the electrochemical performances of the cells in H_2 were evaluated firstly. Fig. 4 shows the measured J-V (P) curves of the two types of cells in H_2 in the temperatures ranging from 700 °C to 800 °C. It is clearly seen that the open circuit voltages (OCVs) of the two cells were very close to 1.1 V, implying that the YSZ electrolyte for both cells were densified and the cells were well sealed to the holder. The peak power densities (PPDs) of Ni-YSZ cell in H_2 were 0.84, 1.12 and 1.41 W cm^{-2} at 700 °C, 750 °C and 800 °C, respectively. These performances are comparable to those of the excellent Ni-based anodes reported [27,28]. Conventionally, electrochemically-active sites for the Ni-YSZ anode are limited in the TPBs of the fuel, YSZ and Ni. H_2 electro-oxidation in the anode is mainly comprised of two processes, that is, H_2 diffusion and dissociation processes over the Ni metal, followed by charge transfer over the interface of Ni and YSZ [29]. Therefore, Ni/YSZ junctions play the key role in the electrochemical reaction. As for the L-PBM NPs infiltrated Ni-YSZ, the active L-PBM NPs make the charge transfer process not merely restricted at the Ni/YSZ junctions. The L-PBM NPs can self-conduct the H_2 diffusion and dissociation, and even the charge transfer process, making the L-PBM/YSZ junctions and L-PBM itself the active sites. At the same time, L-PBM also contributes to fast oxygen ion diffusion to the Ni surface so that the electro-oxidation of H species can readily proceed on the Ni surface. For these reasons, the NPs + Ni-YSZ exhibited much better performance in H_2 with the corresponding PPDs increased to 1.05, 1.42 and 1.91 W cm^{-2}

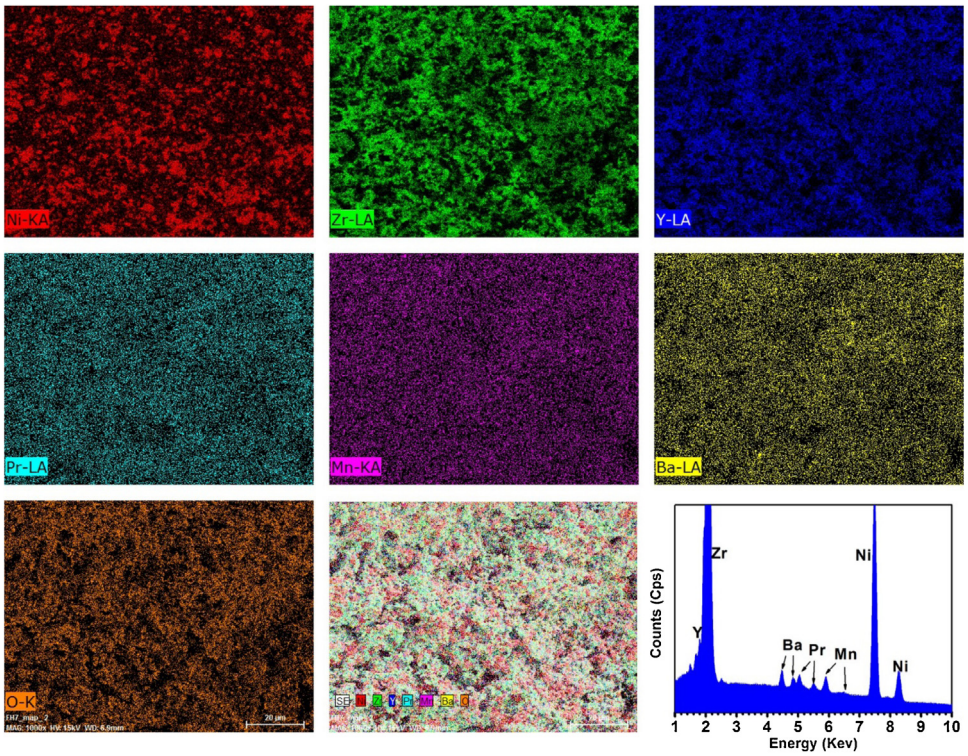

Fig. 3. Cross-sectional microstructure and the energy-dispersive X-ray spectroscopy of the PBM NPs infiltrated Ni-YSZ anode.

at 700 °C, 750 °C and 800 °C, respectively. The two cells exhibited identical ohmic resistance, but the electrochemical polarization resistance of Ni-YSZ cell decreased from 0.61 to 0.34 Ω cm^2 after infiltration of L-PBM NPs (Fig. 4c). The EIS results revealed that the increase of PPDs was mainly contributed to the enhanced electrochemical oxidation process rather than the electronic conductivity.

Although the hybrid anode shows improved electrochemical activity, the carbon deposition resistance and sulfur tolerance are the pivotal factors for this application. Thus, prior to estimating the performance and stability of the cells in biogas, their carbon deposition resistance and sulfur tolerance were compared, respectively. Specifically, H_2-H_2S mixture gas was used to estimate the sulfur tolerance of the cells, while an equal amount of CH_4 and CO_2 was used to estimate the carbon deposition resistance of the cells.

CO_2 and CH_4 are the main components of the biogas, and to the best of our knowledge, $CO_2 + CH_4$ dry reforming reaction is inclined to cause carbon depositions on the catalysts [28]. Fig. 5a and Fig. 5a dispalys the initial performance of the cells in dry CH_4. Regarding the Ni-YSZ cell, the PPDs were 0.82 and 1.12 W cm^{-2} at 750 °C and 800 °C, respectively. The PPDs increased remarkably to 1.03 and 1.46 W cm^{-2} at 750 °C and 800 °C for the NPs + Ni-YSZ cell. It is understandable that the electrochemical activity of the proposed hybrid anode material would also be enhanced in $CH_4 + CO_2$ due to the increased areas of electrochemically-active sites. Nevertheless, the O^{2-} transported from the cathode can only reach a limited part of the Ni-YSZ anode. It has been reported that the electrochemically-active thickness of a typical Ni-YSZ anode is restricted in the range between 10 and 20 μm near the YSZ dense electrolyte [30]. This may lead to carbon depositions in the anode supported layer.

Unlike the situation in H_2, the chemical activity of anodes for dry reforming reaction also contributed to their performances in dry CH_4. With dry CH_4 as the feed, the conversions of CO_2 and CH_4 through the dry reforming reaction is believed to be significant in the anode support because Ni is a good catalyst for this reaction [31,32]. Consequently, the catalytic activity of the Ni-YSZ and NPs + Ni-YSZ catalysts for DRM reaction were also evaluated in a fixed bed reactor, as described in our previous work [1,8]. It is seen from Fig. 5b that the CH_4 conversions and CO selectivi-

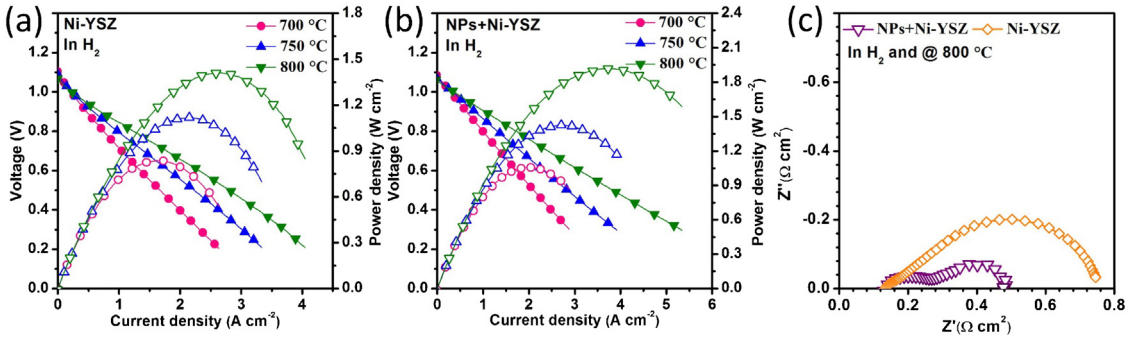

Fig. 4. J-V (P) curves of the cell with Ni-YSZ (a) and PBM NPs infiltrated Ni-YSZ (b) anodes in H_2; (c) electrochemical impedance spectra measured in H_2 at open circuit and 800 °C for Ni-YSZ and NPs + Ni-YSZ cells.

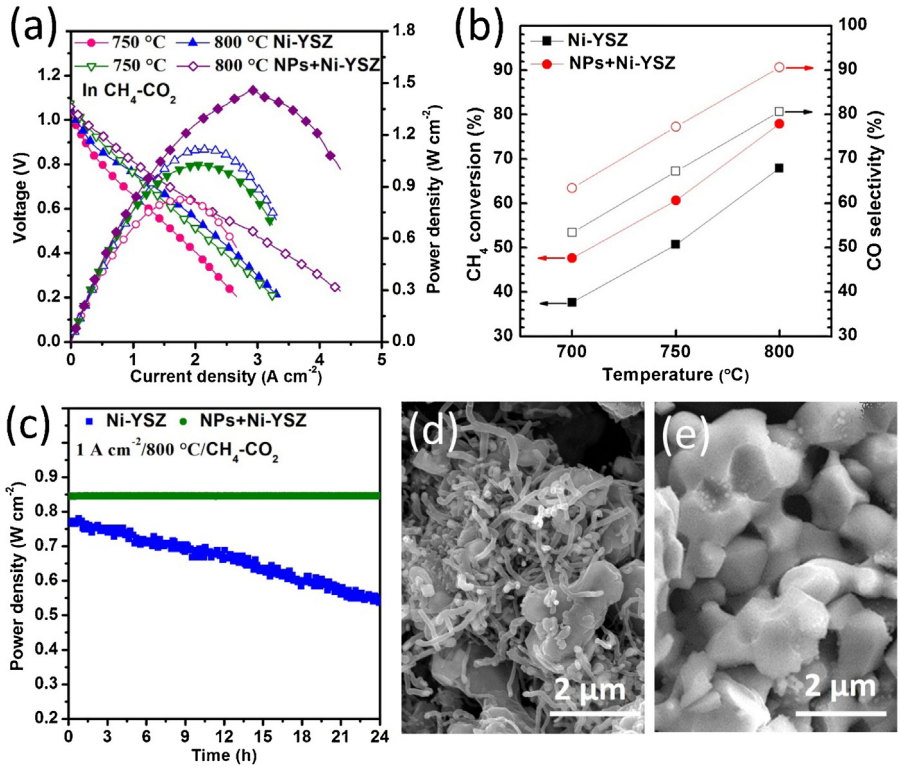

Fig. 5. (a) J-V (P) curves of the Ni-YSZ and NPs + Ni-YSZ cells in dry CH_4 (CH_4:CO_2 = 1:1); (b) CH_4 conversion and CO selectivity of the Ni-YSZ and NPs + Ni-YSZ catalysts; (c) time-dependent voltages of the Ni-YSZ and NPs + Ni-YSZ cells in dry CH_4 (CH_4:CO_2 = 1:1); SEM of the Ni-YSZ (d) and PBM infiltrated Ni-YSZ (e) anodes after test in dry CH_4.

ties of $CH_4 + CO_2$ dry reforming reaction increased rapidly with the increase of temperature for the two catalysts. Except for Ni, perovskite oxides have also been used as the catalysts to launch the CH_4 reforming reaction by many researchers [33]. In our previous study, we have shown the existence of the acid sites on the L-PBM perovskite, which is recognized as a fingerprint for its activity towards the oxidation reaction [13]. Although some active sites on the Ni surface were covered by L-PBM NPs, the NPs + Ni-YSZ catalyst still exhibited better chemical activity than that of the Ni-YSZ catalyst towards $CH_4 + CO_2$ dry reforming reaction (see Fig. 5b). The performance improvement of NPs + Ni-YSZ catalysts can be explained from two aspects. On one hand, L-PBM NPs created additional active sites on the inert YSZ surface; on the other hand, because the mechanisms of DRM over Ni metals and L-PBM oxides are different, the interconnection of the two active sites probably leaded to a synergistic effect to facilitate DRM reaction.

During a prolonged test, the electrochemical behavior of the Ni-YSZ and NPs + Ni-YSZ in dry CH_4 was pronouncedly different. As illustrated in Fig. 5c, the performance of the Ni-YSZ continuously decreased from 0.77 to 0.52 W cm^{-2} in merely 24 h at 1 A cm^{-2} and 800 °C, whereas that of the NPs + Ni-YSZ stabilized at the level of 0.84 W cm^{-2} under the same test condition. A large amount of carbon depositions was present in the Ni-YSZ anode (Fig. 5d), an evidence that the degradation of the Ni-YSZ anode was caused by the carbon formation. On the contrary, no visible carbon species were present in the NPs + Ni-YSZ anode (Fig. 5e), implying that the addition of the L-BPM NPs not only promoted the conversions of CH_4 but also inhibited the formation of the carbon depositions. These could be attributed to the good chemical and electrochemical catalytic activity of L-PBM for hydrocarbon oxidation reactions [13,21].

The sulfur tolerances of the two cells were evaluated in sour H_2. For the Ni-YSZ cell (Fig. 6a), it achieved the PPDs of 0.74 and 1.01 W cm^{-2} at 750 °C and 800 °C in sour H_2. After infiltration of L-PBM NPs, these values were significantly improved to 1.04 and 1.41 W cm^{-2} at 750 °C and 800 °C, respectively. The ratios between the PPDs (at 800 °C) with and without H_2S for Ni-YSZ and NPs + Ni-YSZ were 0.71 and 0.74, respectively. This evidently indicates that initial sulfur tolerance of the Ni-YSZ anode is dramatically improved with the infiltration of 3 wt.% L-PBM NPs. During the long term stability test (Fig. 6b), the Ni-YSZ suffered serious performance degradation. The voltage of the Ni-YSZ dropped from 0.7 W cm^{-2} to 0.54 W cm^{-2} in the 24 h test duration. It is generally accepted that the initial performance degradation is due to the adsorption of S on the Ni surface rather than the formation of nickel sulfites. According to literatures [10], sulfur would adsorb on the nickel surface and along the TPBs, blocking the electrochemically-active sites for fuel oxidation. The S adsorption on Ni surface rapidly achieved the equilibrium and this process was stable and irreversible under the operation conditions. On the contrary, the good performance of NPs + Ni-YSZ maintained during the same test without visible degradation, indicating that the presence of L-PBM NPs inhibited the adsorption of sulfur species and hence substantially reduced the poisoning effect of sulfur on the electrochemical performance of the cell [21]. The SEM-EDX analysis (Fig. 6c and d) of the NPs + Ni-YSZ anode indicated that no sulfur containing species were detected in the anode after test in sour H_2 for 24 h. This evidently supported the speculation that L-PBM NPs inhibited the adsorption of sulfur species.

Finally, we examined the performance and stability of the cells in biogas for practical implementation. The presence of H_2S may alleviate the degree of carbon deposition [34], but the lower electrochemical and chemical activity towards CH_4 oxidation reaction was obtained instead, due to the sulfur poison. Therefore, the Ni-YSZ could can only obtain PPDs of 0.34 and 0.61 W cm^{-2} at 750 and 800 °C, respectively (Fig. 7a). These performances are much lower than those in dry CH_4 and sour H_2. In this case, both the electrochemical and chemical activities of the Ni for CH_4 oxidation

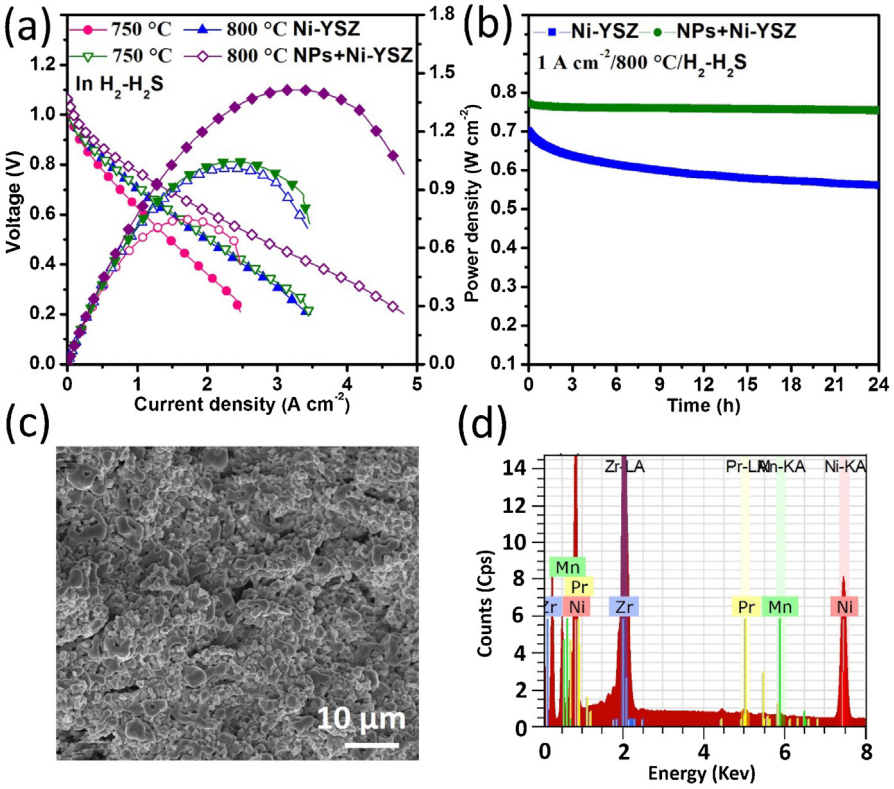

Fig. 6. J-V (P) curves (a) and time-dependent voltages (b) of the Ni-YSZ and NPs + Ni-YSZ cells in sour H_2 (50 ppm H_2S); (c) and (d) SEM-EDX test of the NPs + Ni-YSZ anode after stability test in sour H_2.

were dramatically reduced because of the sulfur poison effect, so the degradation in the initial performance was more pronounced. On the contrary, the NPs + Ni-YSZ yielded similar performance (0.89 and 1.35 W cm^{-2} at 750 and 800 °C, respectively) to those in dry CH_4 and sour H_2, mainly because the L-PBM substantially reduced the poisoning effect of sulfur, as we had well proved previously. In the prolonged test (Fig. 7b), the power density of Ni-YSZ degraded from 0.57 W cm^{-2} to 0.49 W cm^{-2} within 24 h, whereas that of NPs + Ni-YSZ stabilized at around 0.80 W cm^{-2} under the same test duration. Further, a 100 h stability was performed to evaluate the potential of the NPs + Ni-YSZ for co-generating electricity and syngas in the practical application. It is seen from Fig. 7c that the output voltage of the cell stabilized at 0.7 V (1.5 A cm^{-2}) and the biogas was almost transformed into syngas (limited concentrations of CO_2 and CH_4 in the exhausts) that is an important precursor for numerous chemicals [1].

To make a good comparison on the tested Ni-YSZ and NPs + Ni-YSZ anode, SEM and O_2-TPO analysis were performed. Although the activity of Ni-YSZ was severely reduced in biogas, carbon depositions were still detected in the Ni-YSZ anode (tested in biogas for 24 h) by examining the microstructure (Fig. 8a) and O_2-TPO test (Fig. 8c). Both the sulfur poison and carbon formation are responsible for poor performance and stability of Ni-YSZ anode in biogas. Once again, the function of L-PBM NPs was confirmed by examining the microstructure (Fig. 8b) and O_2-TPO test (Fig. 8d) because no carbon depositions were observed and detected in the NPs + Ni-YSZ anode. As schematically shown in Fig. 8e and f, both the carbon formation and S adsorption on Ni were resisted by these NPs. Firstly, these L-PBM NPs are not as active as Ni, so we speculated the formation energy of carbon and adsorption energy of S on the Ni + NPs surface were higher than those on Ni surface. Secondly, the Ni catalyst is much easier to cause carbon deposition

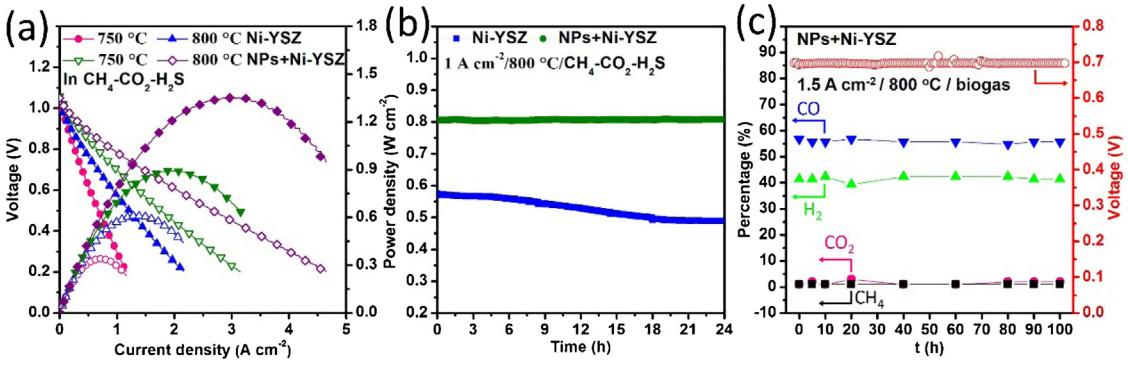

Fig. 7. J-V (P) curves (a) and time-dependent voltages (b) of the Ni-YSZ and NPs + Ni-YSZ cells in dry-sour CH_4 (CH_4:CO_2 = 1:1, 50 ppm H_2S); (c) the time-dependent voltages and the corresponding effluent gas compositions of NPs + Ni-YSZ cells in dry-sour CH_4 (CH_4:CO_2 = 1:1, 50 ppm H_2S) at 800 °C and 1.5 A cm^{-2} during a 100 h stability test.

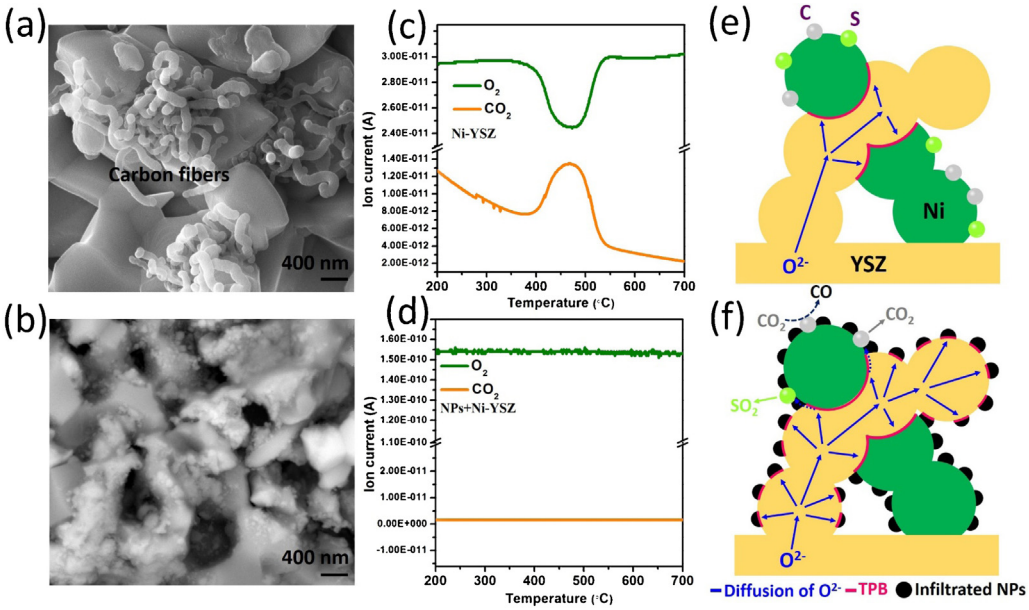

Fig. 8. SEM of the cell with Ni-YSZ (a) and NPs + Ni-YSZ (b) anodes after test in dry-sour CH_4; O_2 and CO_2 signals during the temperature programmed oxidation tests for the Ni-YSZ (c) and NPs + Ni-YSZ (d) cells after test in dry-sour CH_4; (e) and (f) the proposed mechanisms show that the infiltrated NPs not merely resist the deposition of S/C species but also promote the S/C removal process.

and be poisoned by sulfur than L-PBM catalyst. The infiltration of L-PBM NPs reduces the total area of the exposed Ni surface. Thus, both the carbon deposition resistance and sulfur tolerance were significantly improved since the active Ni surface was reduced. Thirdly, the manganite would facilitate the CO_2 adsorption process [35,36], improving both the DRM reaction and the oxidation of the deposited carbons ($C + CO_2 = 2CO$). Finally, the L-PBM has mixed-valence transition metal cations ($Mn^{4+}/Mn^{3+}/Mn^{2+}$) and fast oxygen ion diffusion channels. Because of these features, the L-PBM NPs can also serve as the oxygen sources as well as the mediums for O^{2-} diffusion to accelerate both the carbon removal and S desorption processes. We have, therefore, successfully developed a very promising hybrid anode for direct biogas SOFC.

4. Conclusions

To directly utilize the biogas in SOFC, a hybrid anode material which combines the merits of the conventional Ni-YSZ cermet and the alternative $PrBaMn_2O_{5+\delta}$ perovskite oxide was developed in this study. This perovskite dramatically resisted the carbon formation and S adsorption and at the same time, it also serves as CO_2-captor, and the source and the medium for O^{2-} diffusion to accelerate both the carbon removal and S desorption processes. This hybrid anode, therefore, displayed excellent activity, superior coke/sulfur resistance and stability in biogas, representing a promising technology for the easier and energy-efficient way for direct biogas utilization.

Acknowledgement

This research was financially supported by the Climate Change and Emissions Management Corporation, Alberta, Canada.

References

[1] B. Hua, N. Yan, M. Li, Y. Zhang, Y. Sun, J. Li, T. Etsell, P. Sarkar, K. Chuang, J.-L. Luo, Novel layered solid oxide fuel cells with multiple-twinned $Ni_{0.8}Co_{0.2}$ nanoparticles: the key to thermally independent CO_2 utilization and power-chemical cogeneration, Energy Environ. Sci. 9 (2016) 207–215.

[2] L. Chekli, S. Phuntsho, J.E. Kim, J. Kim, J.Y. Choi, J.-S. Choi, S. Kim, J.H. Kim, S. Hong, J. Sohn, H.K. Shon, A comprehensive review of hybrid forward osmosis systems: performance, applications and future prospects, J. Membr. Sci. 497 (2016) 430–449.

[3] M. Wild, L. O'Neill, T. Zhang, R. Purkayastha, G. Minton, M. Marinescu, G.J. Offer, Lithium sulfur batteries, a mechanistic review, Energy Environ. Sci. 8 (2015) 3477–3494.

[4] S. Yun, P.D. Lund, A. Hinsch, Stability assessment of alternative platinum free counter electrodes for dye-sensitized solar cells, Energy Environ. Sci. 8 (2015) 3495–3514.

[5] Y. Shiratori, T. Ijichi, T. Oshima, K. Sasaki, Internal reforming SOFC running on biogas, Int. J. Hydrogen Energy 35 (2010) 7905–7912.

[6] K. Chen, L. Zhang, N. Ai, S. Zhang, Y. Song, Y. Song, Q. Yi, C.-Z. Li, S.P. Jiang, Feasibility of direct utilization of biomass gasification product gas fuels in tubular solid oxide fuel cells for on-site electricity generation, Energy Fuels 30 (2016) 1849–1857.

[7] L. Dong, M. Asadullah, S. Zhang, X.S. Wang, H.W. Wu, C.Z. Li, An advanced biomass gasification technology with integrated catalytic hot gas cleaning Part I. Technology and initial experimental results in a lab-scale facility, Fuel 108 (2013) 409–416.

[8] B. Hua, M. Li, J.-l. Luo, J. Pu, B. Chi, J. Li, Carbon-resistant Ni-$Zr_{0.92}Y_{0.08}O_{2-\delta}$ supported solid oxide fuel cells using Ni-Cu-Fe alloy cermet as on-cell reforming catalyst and mixed methane-steam as fuel, J. Power Sources 303 (2016) 340–346.

[9] C. Su, Y.B. Chen, W. Wang, R. Ran, Z.P. Shao, J.C. Diniz da Costa, S.M. Liu, Mixed fuel strategy for carbon deposition mitigation in solid oxide fuel cells at intermediate temperatures, Environ. Sci. Technol. 48 (2014) 7122–7127.

[10] Z. Cheng, J.-H. Wang, Y. Choi, L. Yang, M.C. Lin, M. Liu, From Ni-YSZ to sulfur-tolerant anode materials for SOFCs: electrochemical behavior, in situ characterization, modeling, and future perspectives, Energy Environ. Sci. 4 (2011) 4380–4409.

[11] F. Wang, W. Wang, J.F. Qu, Y.J. Zhong, M.O. Tade, Z.P. Shao, Enhanced sulfur tolerance of nickel-based anodes for oxygen-ion conducting solid oxide fuel cells by incorporating a secondary water storing phase, Environ. Sci. Technol. 48 (2014) 12427–12434.

[12] M. Santarelli, F. Quesito, V. Novaresio, C. Guerra, A. Lanzini, D. Beretta, Direct reforming of biogas on Ni-based SOFC anodes: modelling of heterogeneous reactions and validation with experiments, J. Power Sources 242 (2013) 405–414.

[13] Y.-F. Sun, Y.-Q. Zhang, B. Hua, Y. Behnamian, J. Li, S.-H. Cui, J.-H. Li, J.-L. Luo, Molybdenum doped $Pr_{0.5}Ba_{0.5}MnO_{3-(}$ (Mo-PBMO) double perovskite as a potential solid oxide fuel cell anode material, J. Power Sources 301 (2016) 237–241.

[14] S. Cho, D.E. Fowler, E.C. Miller, J.S. Cronin, K.R. Poeppelmeier, S.A. Barnett, Fe-substituted $SrTiO_{3-\delta}$-$Ce_{0.9}Gd_{0.1}O_2$ composite anodes for solid oxide fuel cells, Energy Environ. Sci. 6 (2013) 1850–1857.

[15] M. Li, B. Hua, J.-l. Luo, S.P. Jiang, J. Pu, B. Chi, J. Li, Carbon-tolerant Ni-based cermet anodes modified by proton conducting yttrium- and ytterbium-doped barium cerates for direct methane solid oxide fuel cells, J. Mater. Chem. A 3 (2015) 21609–21617.

[16] M. Li, B. Hua, J.-l. Luo, S.P. Jiang, J. Pu, B. Chi, J. Li, Enhancing sulfur tolerance of Ni-based cermet anodes of solid oxide fuel cells by ytterbium-doped barium cerate infiltration, ACS Appl. Mat. Interfaces 8 (2016) 10293–10301.
[17] P. Zhang, G. Guan, D.S. Khaerudini, X. Hao, C. Xue, M. Han, Y. Kasaie, A. Abudula, Mechanisms of methane decomposition and carbon species oxidation on the $Pr_{0.42}Sr_{0.6}Co_{0.2}Fe_{0.7}Nb_{0.1}O_{3-\delta}$ electrode with high catalytic activity, J. Mater. Chem. A 3 (2015) 22816–22823.
[18] P. Cedric, G. Gilles, R. Pascal, H. Marielle, G. Patrick, V. Rose-Noelle, Synthesis and study of a Ce-doped La/Sr titanate for solid oxide fuel cell anode operating directly on methane, Chem. Mater. 23 (2011) 1539–1550.
[19] S. Suthirakun, S.C. Ammal, A.B. Mun˜oz-García, G. Xiao, F. Chen, H.-C. zur Loye, E.A. Carter, A. Heyden, Theoretical investigation of H_2 oxidation on the $Sr_2Fe_{1.5}Mo_{0.5}O_6$ (001) perovskite surface under anodic solid oxide fuel cell conditions, J. Am. Chem. Soc. 136 (2014) 8374–8386.
[20] S. Choi, S. Sengodan, S. Park, Y.W. Ju, J. Kim, J. Hyodo, H.Y. Jeong, T. Ishihara, J. Shin, G. Kim, A robust symmetrical electrode with layered perovskite structure for direct hydrocarbon solid oxide fuel cells: $PrBa_{0.8}Ca_{0.2}Mn_2O_{5+\delta}$, J. Mater. Chem. A 4 (2016) 1747–1753.
[21] S. Sengodan, S. Choi, A. Jun, T.H. Shin, Y.W. Ju, H.Y. Jeong, J. Shin, J.T. Irvine, G. Kim, Layered oxygen-deficient double perovskite as an efficient and stable anode for direct hydrocarbon solid oxide fuel cells, Nat. Mater. 14 (2015) 205–209.
[22] M.C. Verbraeken, T. Ramos, K. Agersted, Q. Ma, C.D. Savaniu, B.R. Sudireddy, J.T.S. Irvine, P. Holtappels, F. Tietz, Modified strontium titanates: from defect chemistry to SOFC anodes, RSC Adv. 5 (2015) 1168–1180.
[23] Z. Xie, H. Zhao, Z. Du, T. Chen, N. Chen, X. Liu, S.J. Skinner, Effects of Co doping on the electrochemical performance of double perovskite oxide $Sr_2MgMoO_{6-\delta}$ as an anode material for solid oxide fuel cells, J. Phys. Chem. C 116 (2012) 9734–9743.
[24] Z. Liu, B. Liu, D. Ding, M. Liu, F. Chen, C. Xia, Fabrication and modification of solid oxide fuel cell anodes via wet impregnation/infiltration technique, J. Power Sources 237 (2013) 243–259.
[25] D. Ding, X. Li, S.Y. Lai, K. Gerdes, M. Liu, Enhancing SOFC cathode performance by surface modification through infiltration, Energy Environ. Sci. 7 (2014) 552–575.
[26] L. Adijanto, A. Sampath, A.S. Yu, M. Cargnello, P. Fornasiero, R.J. Gorte, J.M. Vohs, Synthesis and stability of $Pd@CeO_2$ core-shell catalyst films in solid oxide fuel cell anodes, ACS Catal. 3 (2013) 1801–1809.
[27] D. Yoon, A. Manthiram, Ni–M (M = Sn and Sb) intermetallic-based catalytic functional layer as a built-in safeguard for hydrocarbon-fueled solid oxide fuel cells, J. Mater. Chem. A 3 (2015) 21824–21831.
[28] J. Ma, C. Jiang, P.A. Connor, M. Cassidy, J.T.S. Irvine, Highly efficient, coking-resistant SOFCs for energy conversion using biogas fuels, J. Mater. Chem. A 3 (2015) 19068–19076.
[29] S.P. Jiang, S.P.S. Bodwal, Hydrogen oxidation at the nickel and platinum electrodes on yttria-tetragonal zirconia electrolyte, J. Electrochem. Soc. 144 (1997) 3777–3784.
[30] A. Enrico, M. Cannarozzo, P. Costamagna, Modeling analysis of Bi-layer $Ni-(ZrO_2)_x(Y_2O_3)_{1-x}$ anodes for anode-supported intermediate temperature-solid oxide fuel cells, Energies 7 (2014) 5647–5674.
[31] C. Guerra, A. Lanzini, P. Leone, M. Santarelli, N.P. Brandon, Optimization of dry reforming of methane over Ni/YSZ anodes for solid oxide fuel cells, J. Power Sources 245 (2014) 154–163.
[32] W. Wang, C. Su, R. Ran, B. Zhao, Z.P. Shao, M.O. Tade, S. Liu, Nickel-based anode with water storage capability to mitigate carbon deposition for direct ethanol solid oxide fuel cells, ChemSusChem 6 (2014) 1719–1728.
[33] F. Mudu, B. Arstad, E. Bakken, H. Fjellvåg, U. Olsbye, Perovskite-type oxide catalysts for low temperature, anaerobic catalytic partial oxidation of methane to syngas, J. Catal. 275 (2010) 25–33.
[34] To. Osaki, T. Horiuchi, K. Suzuki, T. Mori, Suppression of carbon deposition in CO_2-reforming of methane on metal sulfide catalysts, Catal. Lett. 35 (1995) 39–43.
[35] B. Hua, M. Li, B. Chi, J. Li, Enhanced electrochemical performance and carbon deposition resistance of Ni–YSZ anode of solid oxide fuel cells by in situ formed Ni–MnO layer for CH_4 on-cell reforming, J. Mater. Chem. A 2 (2014) 1150–1158.
[36] A. Nandini, K.K. Pant, S.C. Dhingra, K-, CeO_2-, and Mn-promoted Ni/Al_2O_3 catalysts for stable CO_2 reforming of methane, Appl. Catal. A 290 (2005) 166–174.